ARTICLE

High-Directionality Spin-Selective Directing of Photons in Plasmonic Nanocircuits

Received 00th January 20xx,
Accepted 00th January 20xx

DOI: 10.1039/x0xx00000x

Youqiao Ma,*[a] Bo Liu[a], Zhiqin Huang[a], Jinhua Li[a], Zhanghua Han[b],Di Wu[c], Jun Zhou[d], Yuan Ma[e], Qiang Wu[f] and Hiroshi Maeda[g]

Efficient on-chip manipulation of photon spin is of crucial importance in developing future integrated nanophotonics as is electron spin in spintronics. The unidirectionality induced by the interaction between spin and orbital angular momenta suffers low efficiency in classical macroscopic optics, while it can be highly enhanced on subwavelength scales with proper architectures. Here we propose and demonstrate a spin-sorting achiral split-ring coupler to unidirectionally excite dielectric-loaded plasmonic modes in two independent waveguides. We found experimentally that the impinging light with different spin can be selectively directed into one of two branching plasmonic waveguides with a directionality contrast up to 15.1 dB. A circular-helicity-independent compact beam splitter is also realized demonstrating great potential in designing complex interconnect nanocircuits. The illustrated approach is believed to open new avenues for developing advanced optical functionalities with flexible degree of freedom in manipulation of on-chip chirality within chiral optics.

Introduction

Apart from linear momentum, light also carries angular momenta i.e. the spin angular momentum (SAM) and orbital angular momentum (OAM), which respectively determine the polarization and spatial degrees of freedom of photons from a quantum perspective[1]. Over the past few years, the manipulation of coupling between SAM and OAM, known as the spin-orbit interaction (SOI), has been intensively studied owing to their high potential in developing many advanced technologies, such as quantum computing[2,3], chiroptical spectroscopy[4], information processing[5,6], chiral imaging[7,8] and topologic photonics[9-11].

A significant bottleneck for further development is that the spin-orbit coupling is usually very weak at the optical interface inhibiting direct observation through transmitted or reflected light[12]. Surface Plasmon Polaritons (SPPs), on the other hand, which are the electromagnetic waves coupled to electron oscillations and propagating along the interface between metal and dielectrics, hold promise of an unprecedented level in boosting SOI phenomena due to the light confinement far beyond the diffraction limit[13]. Recently, various plasmonic waveguide configurations have demonstrated their remarkable properties of spin-selective control of optical flows in integrated nanocricuits[14-17]. Also, the detection of spin-controlled directional routing has been achieved by achiral plasmonic slot waveguides[18]. Remarkably, the metasurfaces offer a robust opportunity for developing chiral optics with giant photonic spin Hall effect (PSHE), due to the usage of flexible elements and abrupt phase modulation to the reflected and refracted waves[19-21]. Very recently, the on-chip plasmonic spin-Hall nanogratings have also been exploited to simultaneously discriminate both the topological charges and polarization states of the incident beam[22]. However, the metasurfaces and nanogratings are generally realized at the expense of complex configuration and fabrication process, which limits the development of ultracompact photonic spin devices. Miniaturization is the most important feature of next-generation integrated nanocircuits. Developing high-directionality photonic spin devices in subwavelength scale is still a massive challenge.

In this work we demonstrate a dielectric-loaded SPPs (DLSPPs, which is among the most promising configurations for developing plasmonic circuits with relatively low propagation loss and less challenge in fabrication techniques[23]) nanocircuit enabling tunable SOI-controlled unidirectional light routing by an achiral split-ring coupler (SRC). Using the theoretical simulations, we first study the behavior of intrinsic SAM of incident beams coupled to extrinsic OAM of DLSPPs modes within the SRC. It is found that the achiral SRC can selectively couple and direct the DLSPPs flow depending on the spin state of incident radiation. The DLSPPs nanocircuits are then fabricated using electron-beam lithography technique. The

[a] School of Physics and Optoelectronic Engineering, Nanjing University of Information Science and Technology, Nanjing, 210044, China.
[b] Shandong Key Laboratory of Optics and Photonic Devices, School of Physics and Electronics, Shandong Normal University, Jinan 250358, China.
[c] School of Physics and Microelectronics, Key Laboratory of Materials Physics, Ministry of Education, Zhengzhou University, Zhengzhou, Henan 450052, China.
[d] Institute of Photonics, Faculty of Science, Ningbo University, Ningbo 315211, China.
[e] Department of Electrical and Computer Engineering, Dalhousie University, Halifax, NS B3J 2X4, Canada.
[f] Department of physics and electrical engineering, Northumbria University, Newcastle, NE18ST United Kingdom.
[g] Department of Information and Communication Engineering, Fukuoka Institute of Technology, Fukuoka 811-0295, Japan.
* E-mail: mayouqiao188@hotmail.com.
Electronic Supplementary Information (ESI) available.

efficient spin-selective unidirectional wave transfer is experimentally evidenced with most of in-coupled energy directed toward one of the two propagation directions for either left or right circular polarization. The observation of SOI coupling is in accordance with the theoretical predictions. Finally, we also explore the potential applications of the device by symmetrically introducing another two orthogonal DLSPPs waveguides, showing that it not only exhibits the expected unidirectional coupling but also offers the capability in acting as beam splitters under certain circular polarization, which is generally difficult to realize using reported SOI-based devices[14-18]. Our proposed plasmonic device could find direct applications in developing advanced nanocircuits exploiting the spin degree of freedom.

Results and Discussion

Figure 1a schematically shows the proposed on-chip SOI-controlled plasmonic device, which fundamentally provides the working principles. The nanocircuit is composed of two orthogonal DLSPPs waveguides and an achiral SRC containing two identical quarter rings with inner and outer radii of 200 nm and 150 nm, respectively. Under normal incidence, the SRC couples the pump light into one branch of two DLSPPs waveguides, which have sizes of 180 nm in width and 200 nm in height (i.e., the parameters are selected to well balance the trade-off between the mode propagation loss and mode confinement), depending on the handedness of incident light. The excited propagating DLSPPs mode then routes along the DLSPPs waveguide to the end with designed outcoupling grating to scatter the propagating DLSPPs mode out to free space with full control. Figure 1b is the scanning electron microscope (SEM) image of the fabricated sample, in which the inset depicts the zoom on the SRC. The nanocircuits were fabricated on a silver (Ag)-coated silicon (Si) substrate with PMMA ridges as DLSPPs waveguides.

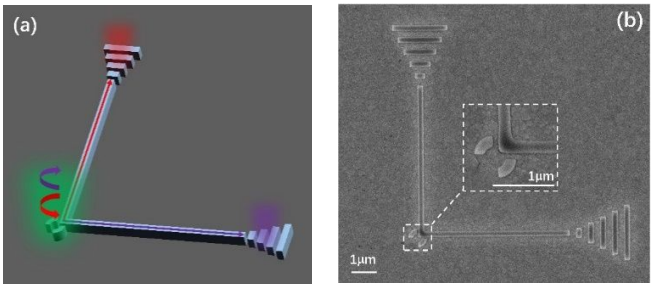

Figure 1. Schematic diagrams of the proposed on-chip spin-controlled unidirectional plasmonic nanocircuit. (a) Three-dimensional (3D) sketch illustrates the left and right circular polarized beams are selectively routed in different DSLPPs waveguide, as annotated with red and purple arrows, respectively. (b) Scanning electron microscopy image shows the top view of the fabricated device. The inset shows the magnified local image of the achiral SRC.

Full 3D finite-difference time-domain (FDTD) simulations were first performed to optimize the structural parameters of the device for effectively sorting the incident radiation according to the state of spin (see Supporting Information S1 for optimization study of SRC geometry). In those simulations, the diffraction-limited optical waves are normally focused on the SRC with respect to the sample surface at the design wavelength of λ = 532 nm, which is selected due to the fact that it is consistent with excitation wavelength of most commonly-used quantum emitters in experiments[24]. From Figure 2a it is clearly observed that, under the left circular polarization (LCP) and right circular polarization (RCP) illumination, the resonant mode is first excited at the SRC and subsequently routes along the corresponding DLSPPs waveguide giving rise to unidirectional energy flow. In other words, when a majority of incident light is coupled into the left (right) branching DLSPPs waveguide, a small part of optical power is in turn directed into the right (left) branching DLSPPs waveguide, leading to a large directionality contrast of □ 15.7 dB, which is evaluated by $10\log_{10}\left(P_1/P_2\right)$, where $P_1$is the power for the desired polarization from one output waveguide, while P_2 is the power for the undesired polarization from the same output waveguide. The underlying mechanism of spin-selective power flow can be understood by the SOI i.e., the spin of incident field couples to the resonant mode within a curved orbit (i.e., split ring) with the extrinsic angular momenta of $\pm hR/\lambda_e$, where h is the Planck constant, R is the inner radius of split ring, and λ_e is the effective wavelength[25]. The handedness of the resonant mode indicated by the sign of '±' determines the direction of coupling to the branching DLSPPs waveguide. To deeply reveal the principles behind SOI phenomena, the optical intensities in individual branching DLSPPs waveguide were calculated and plotted as a function of the illuminating polarization angle. The results are depicted in Figure 2b. We find that the intensities of two branching DLSPPs waveguide are evidently contrast under the LCP (with polarization angle of 90°) and RCP (with polarization angle of 270°) illuminations, while they possess equal intensities for any linear polarization (i.e. LP, with polarization angle of 0, 180° and 360°). This is physically reasonable due to the fact that LP, an equal superposition of LCP and RCP, excites both DLSPPs waveguide equally, so the output intensities of both DLSPPs waveguides is independent on the polarization angle of incident LP beam.

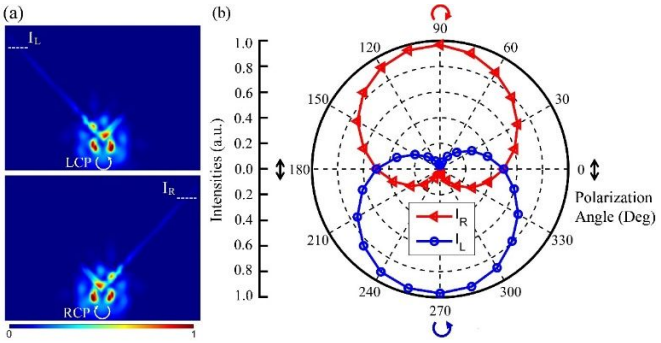

Figure 2. Nanoscale SOI-controlled directional coupler enabling selective excitation of two DLSPPs waveguide modes. (a) Simulated near-field intensity distributions under LCP and RCP incident polarizations revealing unidirectional power guiding along the left and right branching DLSPPs waveguides, respectively. The dashed white lines represent the positions of monitors used for detecting the transmitted intensities through the

waveguides. (b) Output intensities of two branching DLSPPs waveguides versus the incident polarization angles. The angles of 0, 180° and 360° correspond to LP, while the angles of 90° and 270° relate to LCP and RCP illumination, respectively

Now let us consider the experimental verification. We fabricated the proposed DLSPPs devices using electron beam lithography (EBL) and demonstrate spin-selective unidirectional excitation in the fabricated nanocircuits. The geometric parameters of SRC were selected according to above numerical simulations. Fabrication details of the proposed device are given in Methods. Far-field characterization of the fabricated device with two branching DLSPPs waveguides expanding over approximately 6 μm was then conducted by a home-built experimental setup allowing one to image and monitor the scattered far field, where the spin-dependent excitation and analysis were performed utilizing a linear polarizer and a quarter-wave plate (see Methods). An incident beam with a wavelength of 532 nm is focused onto the top of SRC at normal incidence. Part of the incident light is coupled into SRC, and then coupled from the SRC to the branching DLSPPs waveguides. By tuning the orientation of quarter-wave plate relative to the linear polarizer, an incident beam with different polarization states can be generated. Light scattering from outcoupling gratings is monitored in the reflection mode for LCP, RCP and LP states (Figure 3a, b, c). The observed far-field emissions agree well with the spin-sorting functionality theoretically predicted with numerical simulations (Figure 2a). Circularly polarized (CP) light beams with opposite handedness can effectively excite and direct the DLSPPs modes to different waveguide branches, whereas the LP light induces roughly equal intensity profiles at both outcoupling gratings. Importantly, we also find that the emission intensity obtained with the LP incident light is approximately half of those for devices under CP beam illumination. Or in other words, the power scattering from two outcoupling gratings for LP light incidence is coupled to a single outcoupling grating with CP light, confirming the SRC undergoes the SOI process.

To further experimentally illustrate the SOI mechanisms and compare with simulation predictions (Figure 2b), the intensities emitted by two outcoupled gratings were measured for various polarizations of the incident beam (between LP, RCP, LCP and intermediate elliptical polarizations) by rotating the quarter-wave plate from 0 to 360°. The results are depicted in Figure 3d. The measured results under different incident polarization states with opposite directionality are in good agreement with the theoretical results. The incident photons with left and right spin states can be selectively directed to the left and right branching DLSPPs waveguides, respectively. In particular, the average contrast of measured intensities is about 15.1 dB under complete LCP and RCP incidence, verifying the high-directionality of proposed nanocircuits.

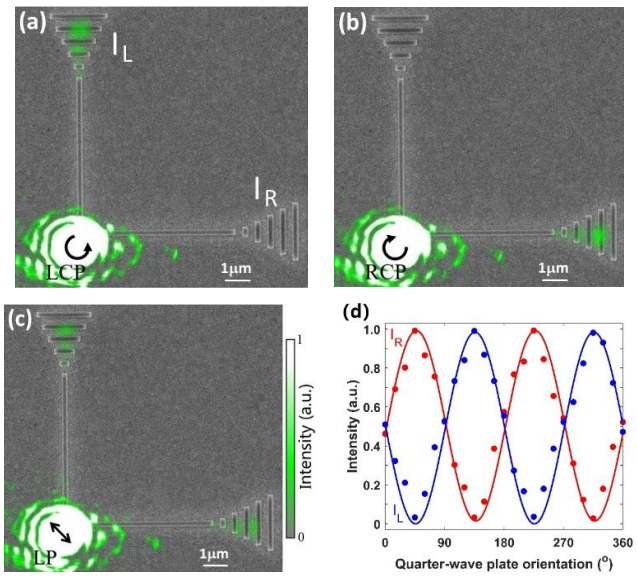

Figure 3. Experimental verifications of SOI-enabled unidirectionality in proposed plasmonic nanocircuits. (a,b,c) Far-field CCD images for device with optimized geometry under LP, RCP and LCP illuminations at wavelength of 532 nm. The states of incident polarization are shown by black arrows. The CCD images are superimposed with the device configuration to indicate the structure's position. (d) Measured emission intensities of two outcoupled gratings as a function of the polarization of incident radiation. The polarization state is controlled by adjusting the orientation of quarter-wave plate with respect to linear polarizer. It varies continuously from LP (0, 90°, 180°) to RCP and LCP (45° and 135°, respectively) with intermediate elliptic states.

Compared with recently reported spin-sorting structures[14-18], the proposed configuration appears to be more prospective in developing advanced interconnect nanocircuits with eliminating the structural reconstruction. Another two orthogonal DLSPPs waveguides, as a most direct demonstration, can be straightforwardly introduced around the second opening to realize the beam splitting functionality after SOI process. We fabricated the nanocircuits containing four DLSPPs outputs with geometric parameters optimized above and imaged the far-field scattering profiles (Figure 4a, b). We find that the DLSPPs mode generated by photons with LCP (RCP) spin is efficiently directed to the two DLSPPs waveguides in vertical (horizontal) direction, which is consistent with that depicted in Figure 3a (Figure 3b). More importantly, the emission intensity of two individual outcoupling gratings under LCP (RCP) illumination is almost identical and half of that obtained in Figure 3a (Figure 3b), due to the symmetric characteristics of structures which enable directing energy from the clockwise circulating mode (i.e., LCP) within SRC equally to the two vertical DLSPPs waveguides with matched momentum, and vice versa. For example, the relative intensities coupled out from gratings I, II, III and IV (as depicted in Figure 4a) under LCP illumination are measured as 0.476, 0.483, 0.0094 and 0.0109, respectively. Therefore, the proposed nanocircuits are capable of splitting the energy by 50/50 without depending on the spin state of CP incidence.

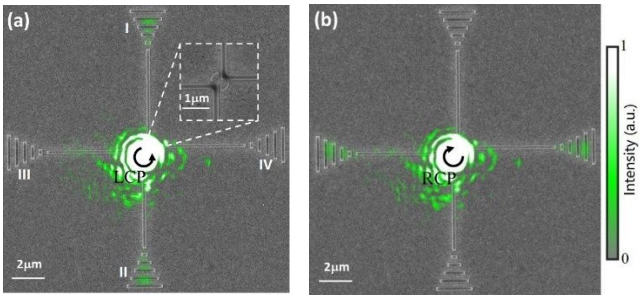

Figure 4. Experimental illustration of SOI-controlled unidirectionality in proposed plasmonic nanocircuits with four branching DLSPPs waveguides. (a,b) Scattering images from the structure observed with (a) LCP and (b) RCP at wavelength of 532 nm. The optical images are superimposed with the structure configuration.

Conclusions

In conclusion, we have proposed and successfully demonstrated a simple plasmonic waveguide nanocircuit for realizing on-chip spin-selective directional routing functionality. Combinations of an achiral split-ring coupler and the orthogonal DLSPPs waveguides enable us to fully control the spin trajectory with a measured directionality contrast amounting to 15.1 dB. The proposed device also enables flexible on-chip interconnect applications by experimentally demonstrating a high-directionality SOI beam splitter. Our work thus may open new perspectives in designing complex spin-optical nanocircuits exploiting manipulation of spin degree of freedom for future nanophotonic technologies.

Methods

Numerical Simulations. All simulated results were obtained by using the finite-difference time-domain method (FDTD) with perfectly matched layer (PML) boundary conditions to absorb the scattered outgoing EM radiations. The nanodevice consists of the PMMA waveguides (n_{PMMA} = 1.49) sitting on the silver substrate, whose wavelength-dependent optical constants were selected based on the experimental data reported by Johnson and Chirsty[26]. Convergence tests were also done to ensure the meshing and boundaries have minimal effect on the solutions. To obtain circular polarization, we employed two 2-μm-diameter linearly-polarized coherent Gaussian beam sources with orthogonal polarizations and a constant phase difference of 90°. The spin states of LP, LCP and RCP can be obtained by adjusting their polarization angles. To obtain the emission intensity, two power monitors were integrated on individual branching DLSPPs waveguide at 3 μm away from the SRC. A profile monitor was parallelly set with silver surface upon 5 nm away to extract the power flow profiles.

Sample Fabrication. The structures were fabricated by multi-step processes including electron beam evaporation coating and electron beam lithography (EBL). First, 3 nm Ti and 100 nm Ag were prepared on Si substrate by electron beam evaporation (DE500C), the Ti film is only used as adhesive layer, the deposition rate of both is 2 Å/s and the pressure in the cavity is 3×10^{-6} Torr. PMMA A4 was coated on the sample at the initial speed of 100 rpm (60 s), and spin-coated on the sample at 3500 rpm (60 s) to obtain 200 nm PMMA coating, baked at 180 ℃ for 90 s to remove the anisole solvent. Then, the pre-designed structure layout was written into a 200 nm thick PMMA coating using a 50 kV electron beam lithography system (Raith VoyagerTM), and the effect of different exposure doses was tested. A sketch of the fabrication process is available in the Supporting Information S2. After development (1:3 MIBK-to-IPA for 30 s followed by 30 s rinse in IPA), scanning electron microscope (SEM) was used to observe the effect of different exposure doses, and the sample parameters under the best exposure dose were selected as the final experimental sample parameters to complete the sample manufacturing.

Optical Measurements. The optical measurements were carried out with a home-built microscope setup. For a sketch of experimental setup, see the Supporting Information S3. A 532 nm continuous-wave pump laser beam is collimated utilizing two lenses with an intermediate pinhole, and its polarization state is adjusted with a linear polarizer coupled to a quarter-wave plate. The pump polarization continuously varies between LP, RCP and LCP by rotating the angle between polarizer and optical axis of quarter-wave plate from 0 to 360°. The incident beam is then tightly focused onto the sample using a 100× (NA 0.90) objective lens passed through a non-polarizing beam splitter. The emitted signal is collected by the same objective and then reflected at the beam splitter to the following CCD camera.

Conflicts of interest

There are no conflicts to declare.

Acknowledgements

The authors would like to thank to financial support from the national Natural Science Foundation of China (Grants No. 61835005, 61822507, 61522501, 11974221), the National Key Research and Development Program of China (Grant No. 2018YFB1800901), and the startup foundation for introducing talent of Nanjing University of Information Science and Technology (NUIST).

Supporting Information

- S1. FDTD simulation and optimization of the geometric parameters under normal and non-normal incidence
  - S1.1 Design optimization of geometry under normal illumination
  - S1.2 Optical response of device under non-normal illumination
- S2. Sample fabrication
- S3. Optical setup utilized for characterization of DLSPPs directionality

References

1 L. Allen, M. W. Beijersbergen, R. J. C. Spreeuw, J. P. Woerdman, *Phys. Rev. A*, 1992, **45**, 8185.
2 P. Lodah, S. Mahmoodian, S. Stobbe, A. Rauschenbeutel, P. Schneeweiss, J. Volz, H. Pichler, P, Zoller, *Nature* 2017, **541**, 473-480.
3 W. B. Gao, A. Imamoglu, H. Bernien, R. Hanson, *Nat. Photonics* 2015, **9**, 363-373.
4 K. W. Smith, L. A. McCarthy, A. Alabastri, L. Bursi, W. S. Chang, P. Nordlander, S. Link, *ACS Nano* 2018, **12**, 11657-11663.
5 X. H. Yin, A. K. U. Michel, A. Tittl, M. Wuttig, T. Taubner, H. Giessen, *Nano Lett.* 2015, **15**, 4255-4260.
6 Q. B. Guo, T. Fu, J. B. Tang, D. Pan, S. P. Zhang, H. X. Xu, *Phys. Rev. Lett.* 2019, **123**, 183903.
7 S. Zu, T. Y. Han, M. L. Jiang, Z. X. Liu, Q. Jiang, F. Lin, X. Zhu, Z. Y. Fang, *Nano Lett*. 2019, **19**, 775-780.
8 Y. Chen, J. Gao, X. D. Yang, *Adv. Optical Mater*. 2019, **7**, 1801467.
9 S. Barik, A. Karasahin, C. Flower, T. Cai, H. Miyake, W. DeGottardi, M. Hafezi, E. Waks, *Science* 2018, **359**, 666-668.
10 N. Parappurath, F. Alpeggiani, L. Kuipers, E. Verhagen, *Sci. Adv.* 2020, **6**, eaaw4137.
11 M. J. Mehrabad, A. P. Foster, R. Dost, E. Clarke, P. K. Patil, A. M. Fox, M. S. Skolnick. L. R. Wilson. *Optica* 2020, **7**, 1690-1696.
12 K. Y. Bliokh, F. J. Rodríguez-Fortuño, F. Nori, A. V. Zayats, *Nat. Photonics* 2015, **9**, 796-808.
13 W L. Barnes, A. Dereux, T. W. Ebbesen, *Nature* 2003, **424**, 824-830.
14 Z. B. Zhang, C. J. Min, Y. N. Fu, Y. Q. Zhang, W. W. Liu, X. C. Yuan, *Opt. Express* 2021, **29**, 6282-6292.
15 Y. Lefier, R. Salut, M. A. Suarez, T. Grosjean, *Nano Lett*. 2018, **18**, 38-42.
16 Y. H. Kan, S. Kumar, F. Ding, C. Y. Zhao, S. I. Bozhevolnyi, *Adv. Optical Mater.* 2020, **8**, 2000854.
17 D. Pan, H. Wei, L. Gao, H. X. Xu, *Phys. Rev. Lett*. 2016, **117**, 166803.
18 M. Thomaschewski, Y. Q. Yang, C. Wolff, A. S. Roberts, S. I. Bozhevolnyi, *Nano Lett*. 2019, **19**, 1166-1171.
19 F. Zhang, M. B. Pu, X. Li, P. Gao, X. L. Ma, J. Luo, H. L. Yu, X. G. Luo, *Adv. Funct. Mater*. 2017, **27**, 1704295.
20 S. M. Chen, K. F. Li, J. H. Deng, G. X. Li, S. Zhang, *Nano Lett*. 2020, **20**, 8549-8555.
21 A. H. Dorrah, N. A. Rubin, A. Zaidi, M. Tamagnone, F. Capasso, *Nat. Photonics* 2021, **15**, 287-296.
22 F. Feng, G. Y. Si, C. J. Min, X. C. Yuan, M. Somekh, *Light Sci. Appl.* 2020, **9**, 95.
23 A. Kumar, J. Gosciniak, V. S. Volkov, S. Papaioannou, D. Kalavrouziotis, K. Vyrsokinos, J.-C Weeber, K. Hassan, L. Markey, A. Dereux, T. Tekin, M. Waldow, D. Apostolopoulos, H. Avramopoulos, N. Pleros, S. I. Bozhevolnyi, *Laser Photonics Rev*. 2013, **7**, 1662.
24 H. Siampour, S. Kumar, V. A. Davydov, L. F. Kulikova, V. N. Agafonov, S. I. Bozhevolnyi, *Light Sci. Appl.* 2018, **7**, 61.
25 D. Marcuse, Light Transmission Optics, Van Nostrand Reinhold: New York, 1972.
26 P. B. Johnson, R. W. Christy, *Phys. Rev*. *B* 1972, **6**, 4370-4379.

Supporting Information for

High-Directionality Spin-Selective Directing of Photons in Plasmonic Nanocircuits

Youqiao Ma,*[a] Bo Liu[a], Zhiqin Huang[a], Jinhua Li[a], Zhanghua Han[b],Di Wu[c], Jun Zhou[d], Yuan Ma[e], Qiang Wu[f] and Hiroshi Maeda[g]

[a.] *School of Physics and Optoelectronic Engineering, Nanjing University of Information Science and Technology, Nanjing, 210044, China.*
[b.] *Shandong Key Laboratory of Optics and Photonic Devices, School of Physics and Electronics, Shandong Normal University, Jinan 250358, China.*
[c.] *School of Physics and Microelectronics, Key Laboratory of Materials Physics, Ministry of Education, Zhengzhou University, Zhengzhou, Henan 450052, China.*
[d.] *Institute of Photonics, Faculty of Science, Ningbo University, Ningbo 315211, China.*
[e.] *Department of Electrical and Computer Engineering, Dalhousie University, Halifax, NS B3J 2X4, Canada.*
[f.] *Department of physics and electrical engineering, Northumbria University, Newcastle, NE18ST United Kingdom.*
[g.] *Department of Information and Communication Engineering, Fukuoka Institute of Technology, Fukuoka 811-0295, Japan.*
* E-mail: mayouqiao188@hotmail.com.

S1: FDTD simulation and optimization of the geometric parameters under normal and non-normal incidence

S1.1: Design optimization of geometry under normal illumination

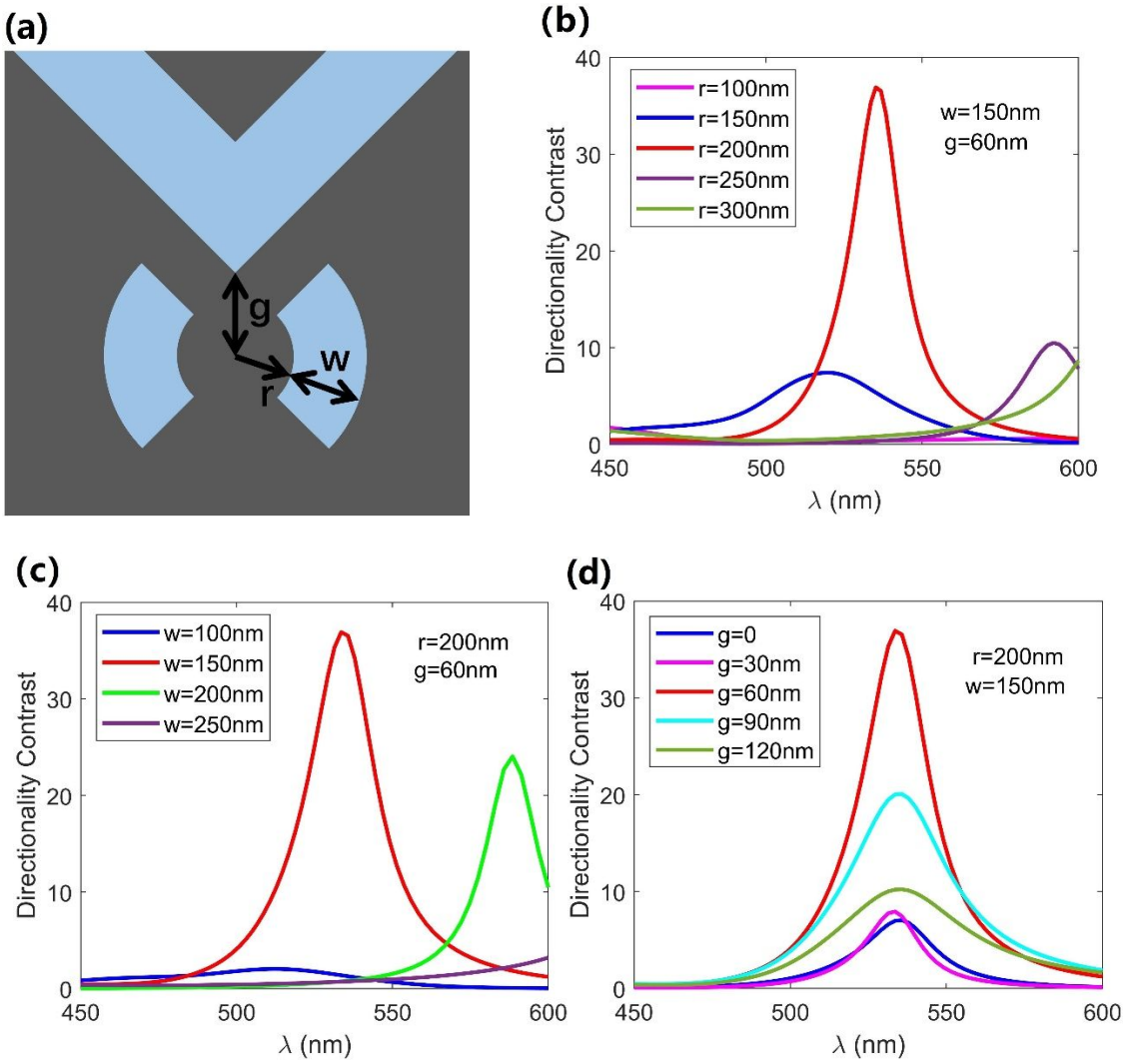

Figure S1.1. 3D-FDTD design optimization of the proposed device for larger directionality contrast between the two branching DLSPPs waveguide channels. The directionality contrast is defined as I_L / I_R under LCP illumination. (a) The top view of the SRC with inner radius of r and width of w. The distance between the center of SRC and the apex of two orthogonal DLSPPs waveguides is noted as g. (b) Directionality contrast as a function of excitation wavelength for different inner radius r while keeping the values of w and g constant as w = 150 nm and g = 60 nm, respectively. Due to the resonant characteristics of SRC, a strong peak is observed at λ = 532 nm for r = 200 nm with a maximum directionality contrast. (c) Directionality contrast as a function of wavelength for different ring width w while keeping r = 200 nm and g = 60 nm reveals the optimal value of w = 150 nm. (d) Directionality contrast as a function of wavelength for device with optimized parameters of r = 200 nm and w = 150 nm while varying the value of g. Due to the fact that the parameters of SRC are fixed, thus the location of resonant peak is almost unchanged.

S1.2: Optical response of device under non-normal illumination

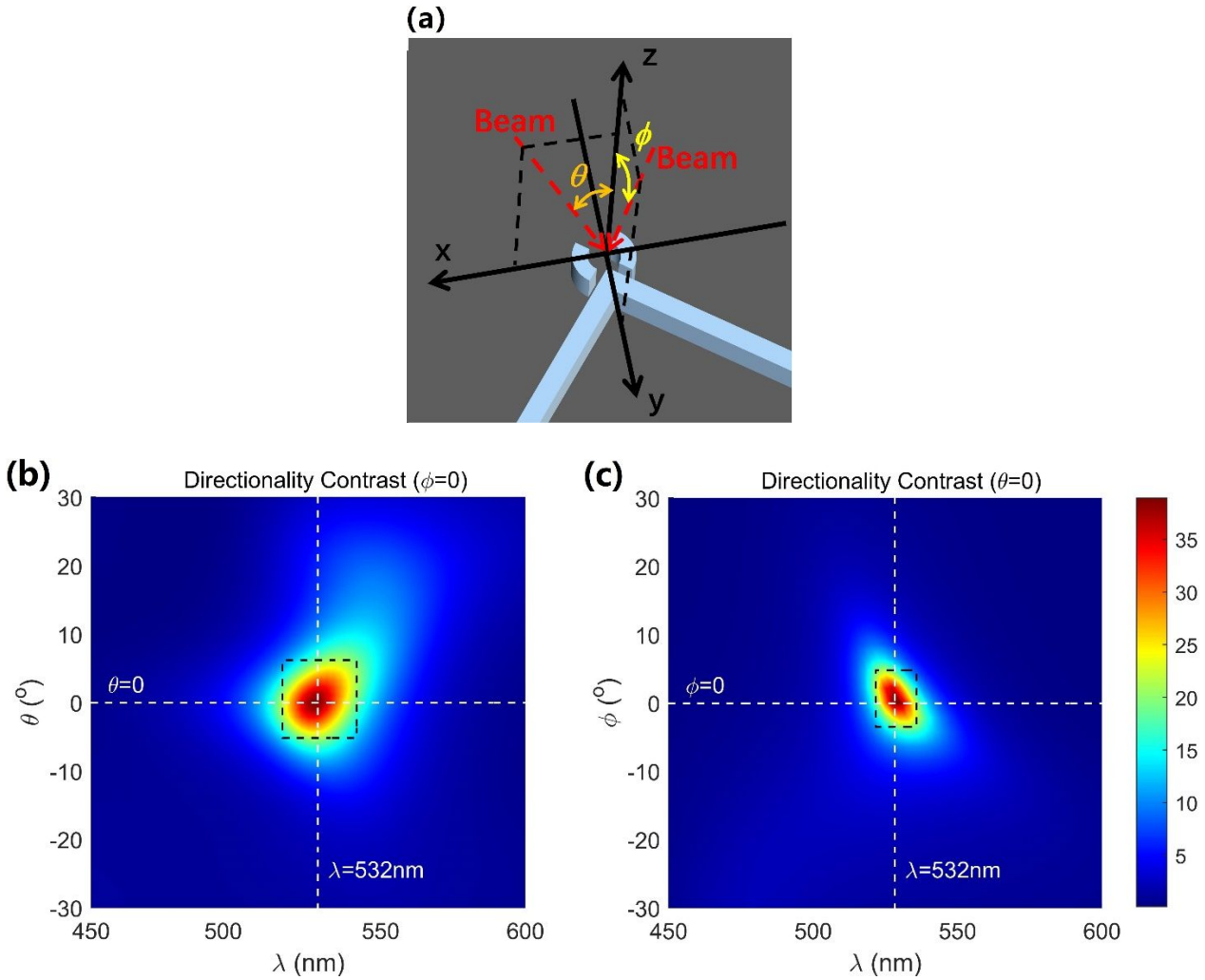

Figure S1.2. 3D-FDTD study of the directionality contrast as functions of both excitation wavelength and nor-normal incident angle. (a) Schematic diagram of the considered coordinate system with respect to the proposed device. We assumed that the beam obliquely shines the device in the x-z plane and y-z plane, with incident angles of θ and ϕ, respectively. (b) Directionality contrast as functions of excitation wavelength and angle θ with $\phi = 0$, which is clearly shown the resonant spectral characteristics for θ varying from -6° to 6°, as shown by the black dashed box. Two dashed white lines indicate the wavelength $\lambda = 532$ nm and incident angle $\theta = 0$. (c) The influence of excitation wavelength and angle ϕ on directionality contrast with $\theta = 0$. Same phenomenon is observed. The results demonstrate the proposed nanocircuit possesses a strong tolerance against the tilted incident angles within ± 5° in x-z and y-z planes ensuring a high average directionality contrast over 25.

S2: Sample fabrication

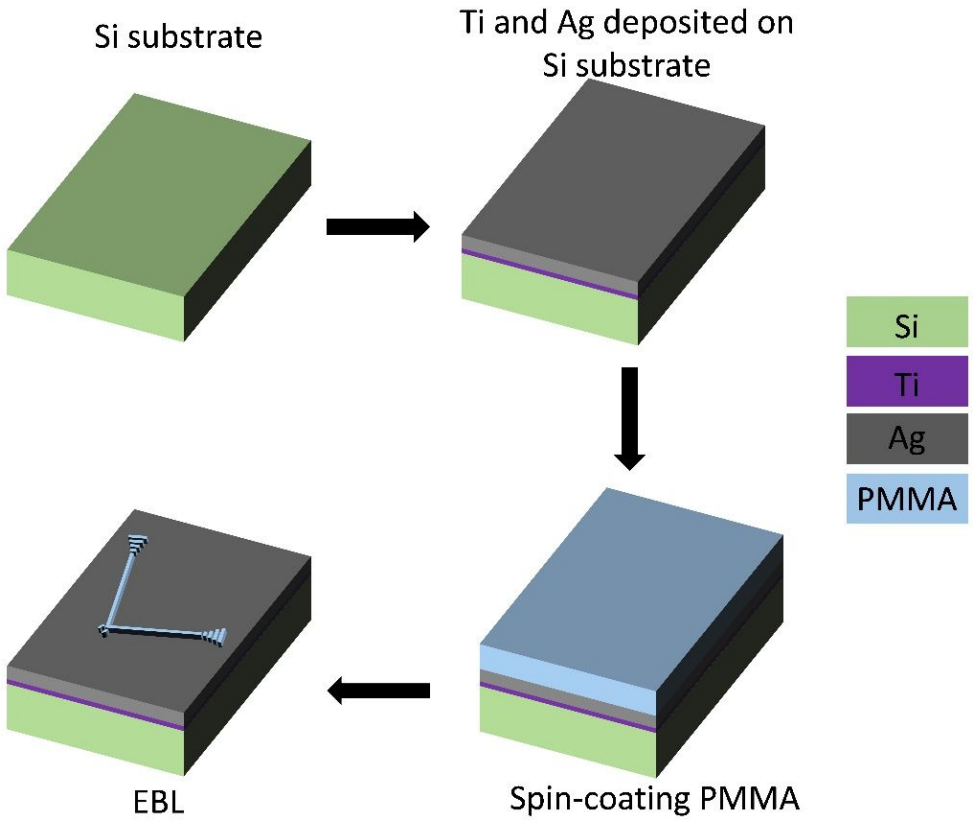

Figure S2.1. Fabrication process of the samples. The Ti and Ag films are successively deposited on the Si substrate. The structured Ag surface is then covered by a PMMA layer using spin-coating, and then the samples are prepared utilizing EBL.

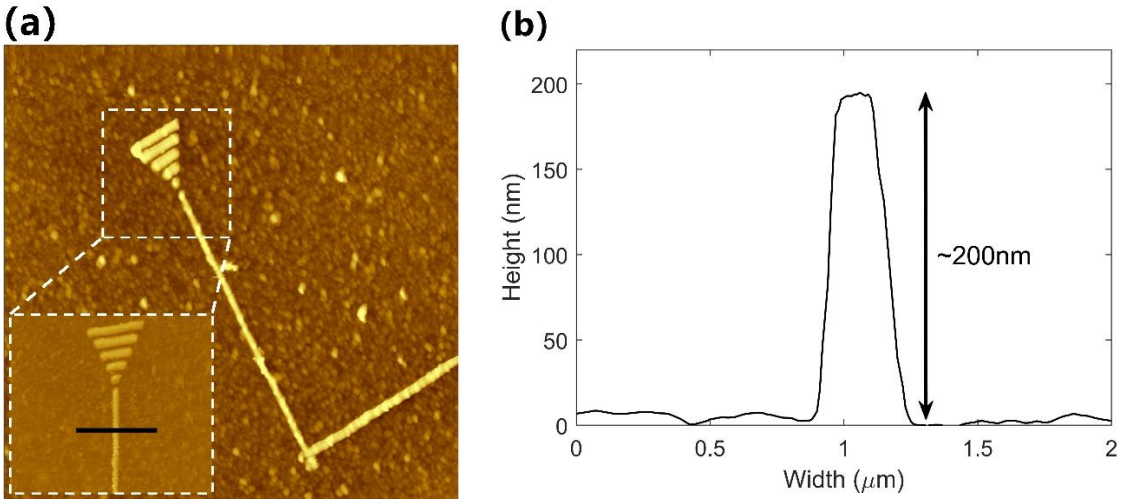

Figure S2.2. (a) The atomic force microscopy (AFM) image of the fabricated sample. (b) The height profile across the blackline depicted in the inset of (a), validating the fabrication precision.

S3: Optical setup utilized for characterization of DLSPPs directionality

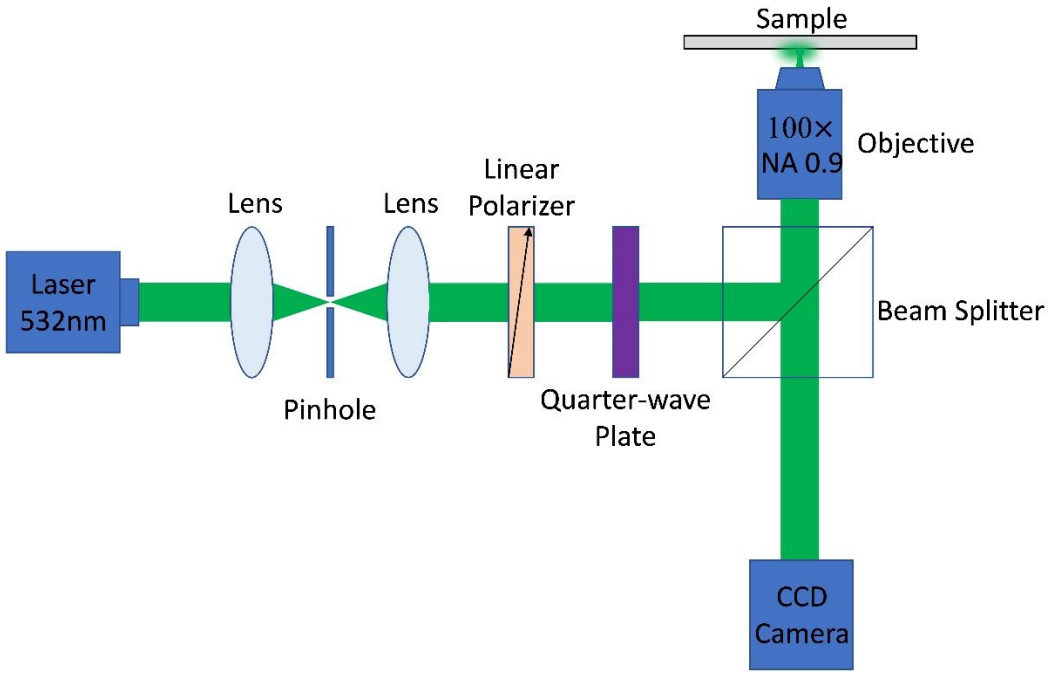

Figure S3. Experimental setup for characterizing emission properties of samples. A 532 nm laser beam is collimated by a set of lenses and pinhole, and passes a linear polarizer and a quarter-wave plate, resulting in continuously varied polarization states between LP, RCP and LCP by adjusting the orientation angle of quarter-wave plate with respect to linear polarizer. Afterwards, the beam is tightly focused onto the sample by an objective. The reflected signal is imaged onto a CCD camera.